Journal of Catalysis **210,** 160–170 (2002)
doi:10.1006/jcat.2002.3660

# *In Situ* ATR–IR Study of the Adsorption of Cinchonidine on $Pd/Al_2O_3$: Differences and Similarities with Adsorption on $Pt/Al_2O_3$

D. Ferri, T. Bürgi,[1] and A. Baiker

*Laboratory of Technical Chemistry, Swiss Federal Institute of Technology, ETH Hönggerberg, CH-8093 Zurich, Switzerland*

Received February 7, 2002; revised April 18, 2002; accepted April 18, 2002

**$Pd/Al_2O_3$ model catalysts have been prepared by physical vapour deposition and characterised by means of XPS, STM, and *in situ* ATR–IR spectroscopy. Morphological changes in the Pd film induced by dissolved hydrogen leads to enhanced infrared absorption and could be followed with both STM measurements and IR spectroscopy. Adsorption of CO, pyridine, quinoline, 2-methylquinoline, and the chiral auxiliary cinchonidine has been studied *in situ* at 283 K in $CH_2Cl_2$ solvent. Two different species have been observed for cinchonidine on Pd. One is oriented with the quinoline moiety nearly parallel to the Pd surface, likely through the $\pi$-system, whereas in the second the $\sigma$-bonding through the *N* lone pair prevails and induces a tilting of the ring with respect to Pd. No indication of the presence of $\alpha$-quinolyl species has been found, in contrast to adsorption on $Pt/Al_2O_3$ catalysts. Compared to adsorption on Pt, cinchonidine is more weakly bound on Pd under hydrogenation conditions. Also, the relative stability of the $\pi$- and *N* lone pair-bonded species is different for the two metals, with the $\pi$-bonded species being relatively more stable on Pt. Similarities and differences found in the adsorption of the chiral modifier on the two metals are discussed and traced mainly to the different d-orbital diffuseness of Pd and Pt.** 

*Key Words: in situ* **ATR–IR spectroscopy; cinchonidine adsorption; palladium; platinum; chiral modification; solid–liquid interface; surface cleaning; enhanced infrared absorption effect.**

## INTRODUCTION

The use of Pd catalysts in industrial applications has grown steeply in recent years due to their practical advantages over platinum. Besides catalytic total oxidation for exhaust emission control (1), heterogeneous palladium-based catalysts are nowadays used in fine chemical synthesis in hydrogenation, hydrogenolysis, and dehydrogenation reactions, and in a number of other relevant chemical transformations (2). Regarding heterogeneous asymmetric catalysis recent work has been reported for the enantioselective hydrogenation of C=C bonds of alkenoic acids (3–6) and pyrones (7–9) with remarkable enantiomeric excess (*ee*). Chiral modifiers such as *cinchona* and to a lesser extent *vinca* (10) alkaloids are employed for inducing chirality in the product. Although working models have been elaborated, there is lack of knowledge on the molecular level of several features relevant to the reaction mechanism. This is mainly due to the intrinsic complexity of the system.

In contrast to the existing attempts to gain insight into the adsorption mode of the modifier under UHV conditions (11–13), we have recently reported the use of *in situ* attenuated total reflection (ATR) IR spectroscopy for investigating the adsorption behaviour of cinchonidine, the most typical modifier, on a $Pt/Al_2O_3$ model catalyst at 283 K (14, 15).

The ATR–IR technique (16) permits adsorption to be monitored *in situ* in the presence of hydrogen and a solvent, i.e., under hydrogenation conditions. The adsorption process on Pt revealed both coverage and time dependence for cinchonidine. At least three species could be identified from the evolution of the ATR signals, corresponding to (i) a nearly flat $\pi$-bonded species (called species **1** in Ref. (15)), (ii) a tilted *N* lone pair-bonded species (**3**), and (iii) a species where the hydrogen atom in $\alpha$-position to the quinoline *N* has been abstracted ($\alpha$-quinolyl-like; **2**). Only the flat and the $\alpha$-quinolyl species appeared strongly bonded to the metal surface, whereas the tilted cinchonidine was weakly adsorbed. Species **1** was also inferred to be the crucial species for catalysis. Cinchonidine adsorption onto Pt foils was also reported independently using reflection–absorption IR spectroscopy (17). A similar transition from flat to tilted adsorption was reported (not mentioning species **2**) in $CCl_4$ but surprisingly at a much higher cinchonidine concentration.

Proposed mechanistic models assume that cinchonidine adsorbs with the aromatic moiety almost parallel to the metal surface on platinum (18). The adsorption on Pd is believed analogous. Although very recently quinoline adsorption has been investigated on Pd(111) by Lambert and co-workers (19), none of the *cinchona* alkaloids has been tested so far on Pd, either under UHV or under reaction conditions. Therefore, to the best of our knowledge, this is the first report on the adsorption of cinchonidine onto palladium. In the first part of this study we focus on the characterisation of the supported Pd model catalyst, similarly to

[1] To whom correspondence should be addressed. Fax: +41 1 632 11 63. E-mail: buergi@tech.chem.ethz.ch.



0021-9517/02 $35.00

that done for the $Pt/Al_2O_3$ model catalyst (20). Then, the adsorption of cinchonidine and model compounds on Pd at 283 K in the presence of hydrogen is described. Finally, differences and similarities between adsorption on Pd and Pt are discussed.

## EXPERIMENTAL

### *Materials*

Cinchonidine (Fluka, 98%), quinoline (Fluka, ≥97%), pyridine (Fluka, ≥99%) and 2-methylquinoline (Aldrich, 97%) were used as received. Dichloromethane solvent (Baker) was stored over 5-Å molecular sieves. $N_2$ (99.995 vol%) and $H_2$ (99.999 vol%) were supplied by PANGAS, whereas CO (0.5 vol% in argon) was supplied by Sauerstoffwerk Lenzburg. Pt (99.99%) and Pd (99.95%) wires and $Al_2O_3$ (99.3%) tablets used as targets for electron beam physical vapour deposition (EB–PVD) were supplied by Unaxis Materials. Trapezoidal Ge internal reflection elements (IRE, Portmann Instruments) were coated by EB–PVD with 100 nm $Al_2O_3$ and then with 1 nm Pt or 2 nm Pd for the ATR–IR spectroscopy (20).

### *Thin Film Characterisation*

The $Pd/Al_2O_3$ thin film was characterised by X-ray photoelectron spectroscopy (XPS) and scanning tunneling microscopy (STM) as previously reported for the Pt and $Pt/Al_2O_3$ thin films (20). STM images were recorded before and after $H_2$ cleaning in order to investigate the effect of hydrogen on the surface morphology. A fragment of coated Ge (1 cm × 1 cm) was contacted with $N_2$-saturated $CH_2Cl_2$ for 2 h and with $H_2$-saturated $CH_2Cl_2$ for 30 min in order to mimic an ATR–IR experiment (see next paragraph).

### *In Situ ATR–IR Spectroscopy*

*In Situ* ATR spectra of the solid–liquid interface were recorded on a Bruker IFS/66 spectrometer equipped with a liquid nitrogen-cooled HgCdTe detector by coadding 200 scans at 4-$cm^{-1}$ resolution. Time-resolved measurements were also performed by coadding 120 scans at a rate of ~11 scans/s. Spectra are presented in absorbance units. A homemade stainless steel flow-through cell equipped with cooling jackets was used. All experiments were performed at 283 K. The experimental protocols have been described elsewhere (15, 20). Briefly, when the metal surface was cleaned before adsorption, $N_2$-saturated solvent was contacted for about 2 h (for signal stabilisation) with the $M/Al_2O_3$ ($M$ = Pt, Pd) thin film followed by $H_2$-saturated solvent for 10 min in order to clean the surface by removing the contamination layer present on the metal. The last spectrum during cleaning served as reference spectrum. Then, adsorption of CO or of the probe molecule at the desired concentration in $CH_2Cl_2$ was carried out. For cinchonidine, quinoline, 2-methylquinoline, and pyridine the solution was saturated with $H_2$. Subsequent to the adsorption step, $H_2$-saturated solvent was allowed to flow through the cell (desorption step). When the cleaning step was not required, as in the case of CO adsorption on untreated Pd, the adsorption step directly followed the signal stabilisation. The solvent saturated with a gas is referred to in the following by the name of the gas, for simplicity.

## RESULTS

### *Characterisation of the $Pd/Al_2O_3$ Model Thin Film*

*XPS and STM.* The XPS spectrum of the deposited 2-nm film of palladium on $Al_2O_3$ exhibited the typical doublet of the Pd 3d level at 340.4 and 355.2 eV. These values correspond to those generally accepted for bulk Pd (21, 22) and indicate that the evaporated Pd film is in the metallic state. Only a small fraction of PdO may be present, as suggested by the asymmetry of the signals, each exhibiting a shoulder on the high-energy side. On the other hand, the XPS line of C 1s displayed a shoulder at ~288 eV, which is assigned to carbonate-like contaminants, as reported also for the Pt film (20). Carbonates (from atmospheric $CO_2$) and water contaminants are expected to be present on the surface due to the exposure of the thin film to air following the vacuum deposition.

The STM images of the $Pd/Al_2O_3$ film before and after $H_2$ treatment are shown in Fig. 1 and demonstrate the reconstruction of the metal film induced by admission of hydrogen. The samples shown belong to the same vapour deposition batch, but Fig. 1A was measured as deposited, whereas Fig. 1B was imaged after treatment in $N_2$ and $H_2$, as described above. It must be noted that the same tip was used to record the two images, that several regions of both samples were scanned, and that all presented similar features. Figure 1A depicts small round particles about 8 nm in size, which we assign to Pd. The STM image of the $Al_2O_3$ underlayer does not exhibit these features (20). The particle size distribution appears rather homogeneous. Figure 1B shows that rather large particles (ca. 15–20 nm) are formed subsequent to the $H_2$ treatment. These larger particles coexist with smaller ones, resulting in a more heterogeneous particle size distribution. Morphological changes induced by hydrogen (and oxygen) have been reported for evaporated Pd-based model catalysts (23, 24). Similar surface modification has also been observed for the $Pt/Al_2O_3$ model catalyst treated with CO and $H_2$, as previously described (20). The morphology of the metal surface plays a crucial role in surface-enhanced infrared absorption.

*Surface cleaning.* The effect of the $H_2$ treatment on the metal surface was investigated by *in situ* ATR–IR spectroscopy. We have recently shown that this treatment is necessary to generate domains of clean Pt (20). After a signal stabilisation period of about 2 h under a $N_2$ stream,

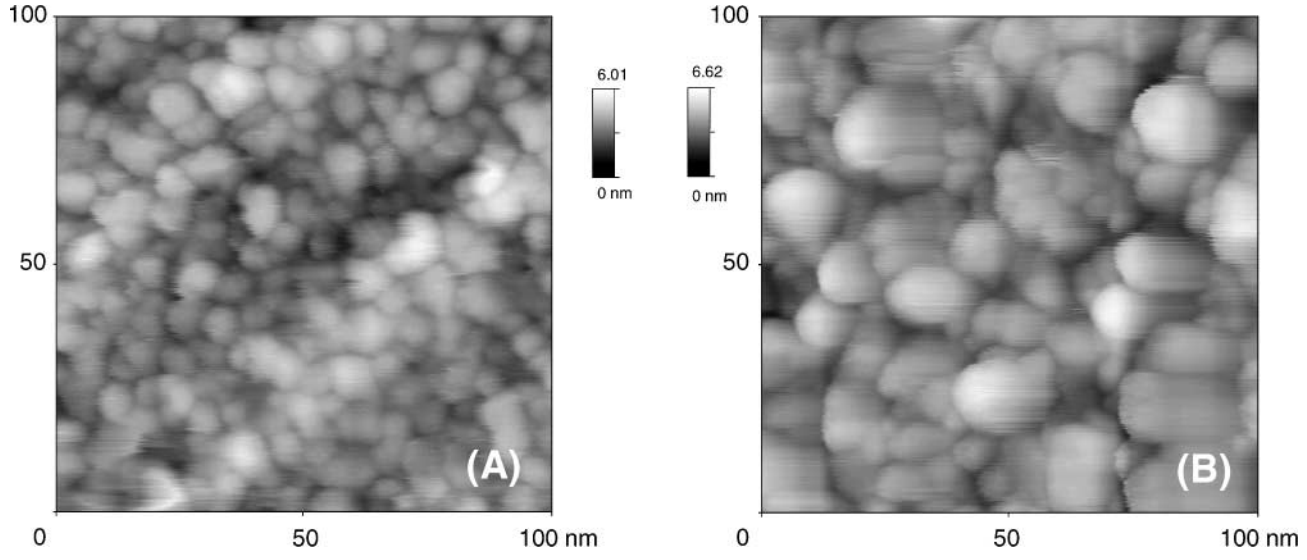


**FIG. 1.** STM images (scan area, 100 nm × 100 nm) of $Pd/Al_2O_3$-coated Ge fragments (1 cm × 1 cm) before (A) and after (B) $H_2$ treatment at room temperature.

the metal surface was contacted with $H_2$ for 30 min, exactly the amount of time used for the treatment of the coated Ge fragment shown in Fig. 1B. The results are shown in Fig. 2, where *in situ* ATR spectra collected at 5-min intervals are depicted in the 1900- to 1100-$cm^{-1}$ spectral range. The negative signals found at 1631 and 1527 $cm^{-1}$ are assigned to the hydrogen-induced removal of carbonate-like species, as was previously observed in the case of the Pt thin films. A spectrum recorded during cleaning of a Pt film is also shown in Fig. 2 for comparison. The negative signal at 1264 $cm^{-1}$ is attributed to the incomplete compensation

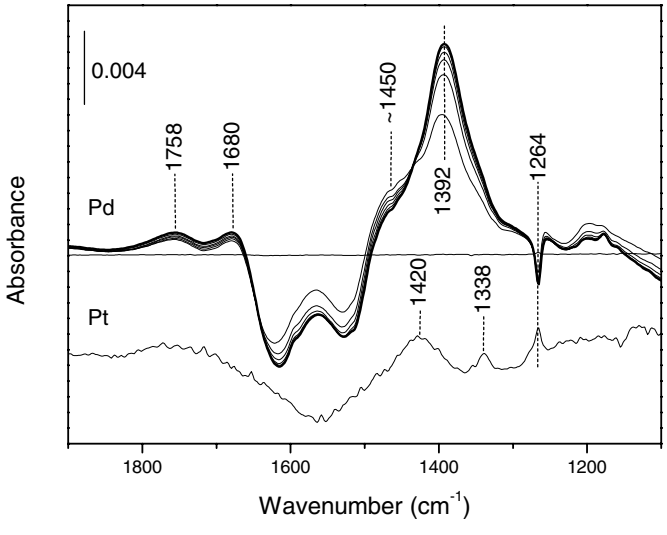


**FIG. 2.** *In situ* ATR–IR spectra of the cleaning of $Pd/Al_2O_3$ and $Pt/Al_2O_3$ films with hydrogen dissolved in $CH_2Cl_2$ at 283 K. Spectra of the $Pd/Al_2O_3$ catalyst were recorded at 5-min intervals. The bold line represents the last spectrum recorded during $H_2$ treatment.

of the most prominent solvent band (14, 20), whereas the signal at 1392 $cm^{-1}$ is ascribed to the formation of hydrocarbon fragments ($CH_x$ hereafter) originating from decomposition of $CH_2Cl_2$ solvent on the Pd surface (25).

Possibly, the band observed at 1455 $cm^{-1}$ belongs to O-containing species due to reaction of adsorbed hydrogen with the contamination layer covering the metal surface. The frequency well agrees with the $\delta$(CH) of alkoxy groups (26).

The weak bands observed at 1758 and 1680 $cm^{-1}$ may arise, despite the surprisingly low position, from adsorbed CO produced by decomposition of the carbonate species. Finally, a reorganisation of the water layer present on the film surface due to the change of the potential at the metal surface upon admission of hydrogen is presumably the origin of the broad signal, extending from 2600 to about 3550 $cm^{-1}$ (not shown), together with a negative signal at ca. 3620 $cm^{-1}$ (27). Thus, some contribution to the negative signal at 1631 $cm^{-1}$ could also arise from adsorbed water.

*Adsorption of CO.* Figure 3A depicts the adsorption of CO on a clean $Pd/Al_2O_3$ thin film. Adsorbed CO exhibits two signals, at 2044 and 1860 $cm^{-1}$, at low coverage. Increasing CO coverage produces an increase in intensity and a blueshift to 2055 and 1869 $cm^{-1}$ (high coverage), respectively. Both signals reach saturation after about 30 min. The shift of the signals is caused by the increasing surface CO concentration and consequently by the increasing extent of dipole–dipole coupling. The rather broad signal at 1869 $cm^{-1}$ is assigned to multibonded CO on Pd, whereas that at 2055 $cm^{-1}$ to linear CO on Pd. For band position and shape our results compare perfectly with previously reported data of CO adsorption from the gas phase on

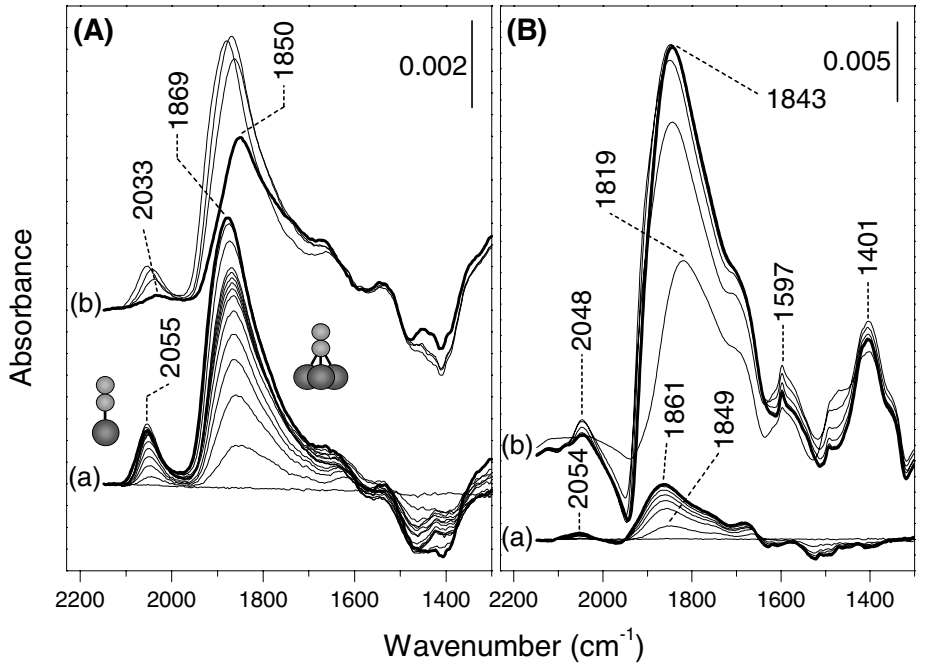


**FIG. 3.** *In situ* ATR–IR spectra of CO adsorption from $CH_2Cl_2$ solvent on $Pd/Al_2O_3$ at 283 K as function of time. (A) Adsorption on clean Pd: (a) spectra recorded during CO adsorption (maximum, 2 h) and (b) spectra recorded during the following $H_2$-saturated $CH_2Cl_2$ flow. Spectra are offset for clarity. The bold lines represent the last spectra recorded in each step. The first 12 spectra of CO adsorption were recorded at 11-s intervals. (B) Spectra recorded during CO adsorption on untreated $Pd/Al_2O_3$ (adsorption time, 30 min) (a) and during the following $H_2$ admission (b). All spectra were recorded in $CH_2Cl_2$ solvent at 283 K. Bold traces represent the last spectra recorded in each step.

evaporated Pd films studied by ATR–IR spectroscopy (28). They also agree with CO on supported and single-crystal Pd surfaces (29, 30).

The following $H_2$ treatment causes attenuation and redshift of the signal corresponding to bridged CO, whereas the signal at 2055 $cm^{-1}$ almost completely disappears. This is due to removal of CO from the metal surface on hydrogen adsorption. The signal centred at 1850 $cm^{-1}$ in Fig. 3 is clearly composed of several bands. Shoulders are distinguished on the high- and low-energy side and can be assigned to different multibonded adsorbed CO species (30). The negative signals detected below 1500 $cm^{-1}$ are assigned to the removal of the hydrocarbon fragments from palladium originating from the cleaning of the surface on admission of $H_2$ (compare with Fig. 2). A band is again observed at ~1680 $cm^{-1}$.

When the metal surface was not cleaned before CO admission, adsorption was considerably slower but the frequencies of adsorbed CO remained rather similar to those reported in Fig. 3A. After a 30-min contact with CO the absorbance of the signal at 1861 $cm^{-1}$ is stabilised. We have reported that hydrogen treatment following CO adsorption on the Pt surface induces an enhancement of the CO signal by a factor of 3–4 (20). The effect was attributed to the reconstruction of the Pt film. Figure 3B clearly shows that the same phenomenon is observed for palladium. Spectra corresponding to traces (b) were collected at 10-min interval. Care was taken that no CO was admitted to the metal surface simultaneously to hydrogen. Thus, the signal increase is associated with the enhancement of the absorbance of already adsorbed CO. An enhancement by a factor of 6–7 is estimated for CO on clean $Pd/Al_2O_3$. Figure 3B also shows that hydrogen induces some changes on the metal surface although CO is already present on palladium. The signal at ~1400 $cm^{-1}$ has to be attributed to decomposition of $CH_2Cl_2$, as reported above. An $H_2$-induced reaction, presumably involving CO, is likely the origin of the sharp signal observed at ~1600 $cm^{-1}$, which was not detected on $Pt/Al_2O_3$.

The change in intensity of the signal of bridged CO is accompanied by a redshift to 1843 $cm^{-1}$ ($\Delta\nu = 25$ $cm^{-1}$), whereas the linearly bonded CO shifts to 2048 $cm^{-1}$ ($\Delta\nu =$ 7 $cm^{-1}$). Moreover, as consequence of $H_2$ admission the strong signal corresponding to bridged CO exhibits a rather strong dispersive shape, with a negative-going high-energy side (Fig. 3B) similar to the behaviour observed and discussed in more detail for the Pt thin films (20). This must be related to changes in the optical properties of the metal film upon reconstruction induced by hydrogen (31), which has been shown by STM (Fig. 1).

*Adsorption of pyridine.* Pyridine is not only another valuable probe molecule for the model catalyst, it also represents a structural component of the alkaloid cinchonidine.

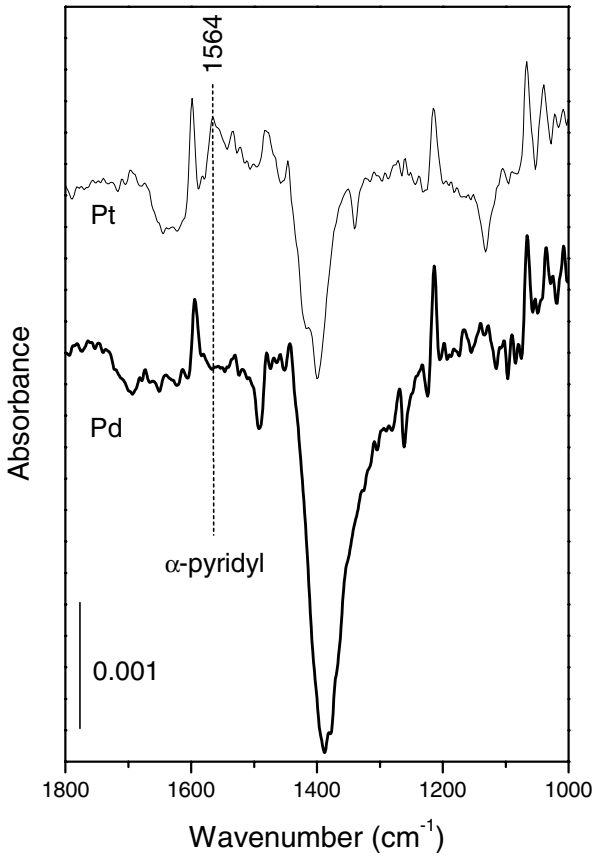


**FIG. 4.** *In situ* ATR spectra of pyridine adsorption from $H_2$-saturated $CH_2Cl_2$ solvent on $Pd/Al_2O_3$ and $Pt/Al_2O_3$ at 283 K. The concentration of the solutions was set at $10^{-4}$ and $10^{-3}$ M for adsorption on Pd and Pt, respectively. The position of the signals corresponding to the $\alpha$-pyridyl species on $Pt/Al_2O_3$ is also highlighted.

Pyridine was adsorbed from a $10^{-4}$ M solution in $CH_2Cl_2$ at 283 K. The ATR spectra of pyridine on $Pd/Al_2O_3$ and on $Pt/Al_2O_3$ at 1800–1000 $cm^{-1}$ are shown in Fig. 4. Signals at 1594, 1479 and 1443 (weak), 1213, 1065, and 1035 $cm^{-1}$ together with a strong negative signal at 1390 $cm^{-1}$ confirmed the adsorption of pyridine on the $Pd/Al_2O_3$ model system. The signals can be attributed to pyridine adsorbed with the molecular plane tilted with respect to the surface (32), and to displacement of hydrocarbon fragments (band at 1390 $cm^{-1}$), as described for $Pt/Al_2O_3$ (14). Another signal was detected at ~1540 $cm^{-1}$, which will be assigned later.

All signals corresponding to adsorbed pyridine disappeared with the following hydrogen flow, indicating that adsorption is rather weak, which well agrees with a pyridine–metal interaction through the lone pair of the *N* atom. Figure 4 clearly shows that no signal corresponding to a species arising from $\alpha$-H abstraction could be detected on Pd, in perfect agreement with the fact that the $\alpha$-pyridyl species has been observed on several noble metals (33–37) *except* palladium (38). Apart from the signal at 1564 $cm^{-1}$ observed on Pt and assigned to $\alpha$-pyridyl, the signals of pyridine on the two metals largely agree. Only the signals at 1594 and 1065 $cm^{-1}$ on Pd are found at slightly lower frequencies ($\Delta\nu = 4$ and 3 $cm^{-1}$, respectively) compared to Pt.

### *Adsorption of Cinchonidine on $Pd/Al_2O_3$*

The *in situ* ATR spectra of cinchonidine on $Pd/Al_2O_3$ at 283 K are presented in Fig. 5 as a function of time. The adsorption was carried out from a $10^{-4}$ M solution in $CH_2Cl_2$ solvent, in presence of hydrogen. The adsorption of cinchonidine on $Pt/Al_2O_3$ under the same conditions is also shown for comparison. We have previously reported that cinchonidine could not be detected on the bare $Al_2O_3$ film (15). Therefore, it is assumed that the signals observed in the presented ATR spectra belong to cinchonidine adsorbed on the metal surface. Table 1 gives the ATR signals in the 1650- to 1450-$cm^{-1}$ spectral range obtained on Pt and Pd together with the assignment (15). For comparison the signals of cinchonidine in solution are also reported.

In the early stages of adsorption on Pd no clear signal belonging to cinchonidine can be distinguished except for

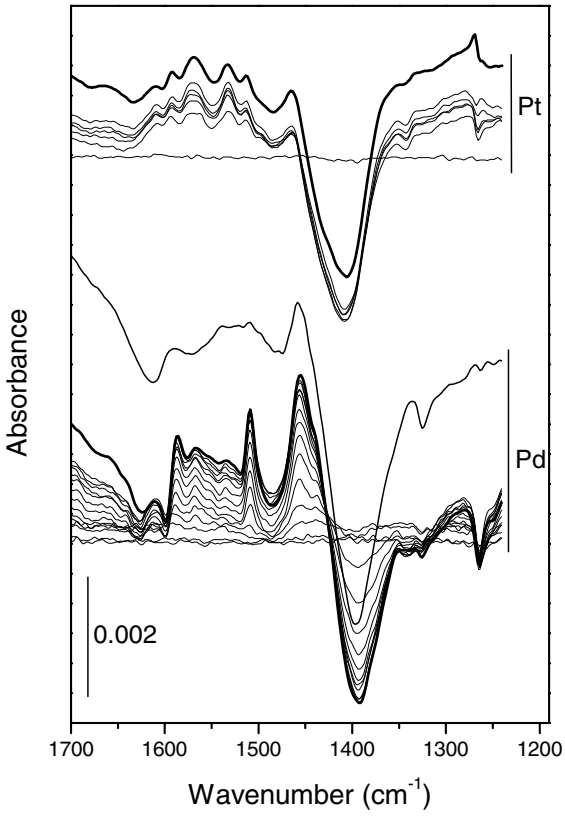


**FIG. 5.** *In situ* ATR spectra of cinchonidine adsorption from $H_2$-saturated $CH_2Cl_2$ solvent on $Pd/Al_2O_3$ and $Pt/Al_2O_3$ at 283 K as a function of time. The bold traces represent spectra at high cinchonidine coverage ($\theta$). For the $Pd/Al_2O_3$ thin film a spectrum recorded during the desorption step is also shown. Spectra of cinchonidine on $Pd/Al_2O_3$ below the bold trace were recorded at 11-s intervals.

**TABLE 1**

**Selected Vibrational Frequencies ($cm^{-1}$) of Cinchonidine in Solution and Adsorbed on $Pt/Al_2O_3$ and $Pd/Al_2O_3$ Model Catalysts at 283 K**

| Assignment | Solution[a,b] | $Pt/Al_2O_3$[b] | $Pd/Al_2O_3$[c] |
|---|---|---|---|
| $\delta$(C–H) | 1454 | 1458[1,2,3] | 1456[1′,3′] |
| Ring stretch | 1463 | | |
| Ring stretch | 1509 | 1511[3] | 1509[3′] |
| $\alpha$-Quinolyl | 1570 | 1530[2] | n.o. |
| Ring stretch | 1570 | 1570[1,2,3] | 1567[1′,3′] |
| Ring stretch | 1593 | 1590[3] | 1586[3′] |
| Ring stretch | 1615 | 1610[3] | 1612[3′] |
| C=C stretch | 1635 | n.o.[d] | n.o. |

[a] IR spectrum of a 0.01 M solution in $CH_2Cl_2$.

[b] See Ref. (15).

[c] This work. **1**, **2**, **3**, **1′**, and **3′** follow the notation for the adsorbed species of cinchonidine (see text).

[d] n.o., Not observed (see text).

that at ~1450 $cm^{-1}$ (quinuclidine (15)) together with the negative band at around 1400 $cm^{-1}$. These two signals indicate that cinchonidine adsorbs on Pd. Then, sharp signals corresponding to the quinoline moiety of the alkaloid appear. The typical signals of cinchonidine can be found at 1612, 1586, 1567, 1509, and 1456 $cm^{-1}$. As in the case of $Pt/Al_2O_3$, the absence of the signal at 1635 $cm^{-1}$ indicates fast hydrogenation of the vinyl group.

Figure 5 shows that the intensity of the signals at 1586 and 1567 $cm^{-1}$ changes with time. In the first spectra the two signals have comparable intensity, whereas in the last spectrum (bold trace) the absorbance of the signal at 1586 $cm^{-1}$ is stronger. From similarity to the Pt model system (14, 15), we assign this behaviour to the presence of at least two different adsorbed species. One of them is related to the signal at 1567 $cm^{-1}$, whereas the second is related to the set of signals at 1612, 1586, and 1509 $cm^{-1}$. Note that the second species also contributes to the signal at 1567 $cm^{-1}$. The two species interact differently with the metal surface.

Only very weak signals at 1589, 1510, and 1458 $cm^{-1}$ remain following the desorption step, together with a broad band around 1539 $cm^{-1}$, which was also observed in the case of CO (Fig. 3A) and pyridine adsorption. Figure 5 shows that adsorption of cinchonidine appears rather weak on $Pd/Al_2O_3$.

Figure 6 presents the *in situ* ATR spectra of cinchonidine adsorbed on Pd at 283 K as a function of solution concentration. The inset of the figure details the behaviour of the absorbance of the signal at 1456 $cm^{-1}$ (full circles) since this signal is common to the observed surface species of cinchonidine. An equal trend has also been observed for the other signals belonging to cinchonidine. For comparison, the inset also reports the calculated line assuming Langmuir adsorption and that absorbance is proportional to coverage. The corresponding behaviour of the signal found on Pt is also given (open circles) (15). A Gibbs free energy of $29 \pm 1$ kJ/mol is calculated from the adsorption isotherm at 283 K by treating the data as for the $Pt/Al_2O_3$ film (15).

In contrast to the adsorption of cinchonidine on Pt, it is not possible to distinguish in Fig. 6 any clear signal attributable to the alkaloid at very low coverage, except for that typical of the quinuclidine moiety at 1456 $cm^{-1}$. As the solution concentration increases, the signals at 1586 and 1567 $cm^{-1}$ grow at different rates. In fact, the absorbance of the former signal increases much more at higher coverage. The signal at 1509 $cm^{-1}$ follows the trend of that at 1586 $cm^{-1}$, as expected on the basis of the results of cinchonidine adsorption on Pt.

From the inset of Fig. 6 the ratio between the absorbance of the quinuclidine signal on Pd and Pt, $A(Pd)_{1456}/A(Pt)_{1458}$, can easily be estimated. The value varies from >4 to ~3 at increasing coverage. This ratio holds also for the other typical signals of the alkaloid, as is evident from Fig. 5. Two reasons for this can be cited. One may deduce that the amount of adsorbed cinchonidine on Pd is larger than on Pt. Conversely, Fig. 3B shows that the CO signals on Pd are enhanced by a factor of about 6–7 when hydrogen is admitted. This enhancement factor is 2–3 times larger than that observed on Pt. Hence, the stronger cinchonidine signals observed on Pd as compared to Pt are attributed mostly to the larger enhancement factor on the former metal.

*Adsorption of quinoline and 2-methylquinoline.* Quinoline and 2-methylquinoline were also admitted onto the

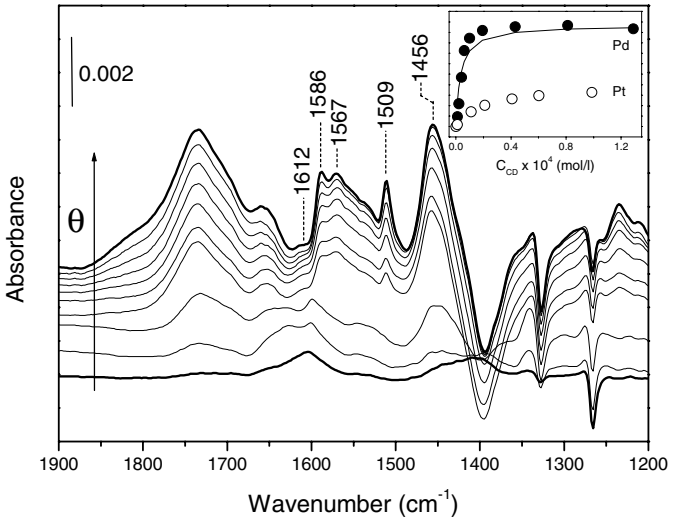


**FIG. 6.** *In situ* ATR spectra of cinchonidine adsorption from $H_2$-saturated $CH_2Cl_2$ solvent on $Pd/Al_2O_3$ at 283 K as a function of cinchonidine concentration in solution. The bold traces represent low and high cinchonidine coverage ($\theta$). The inset shows the absorbance of the signal at 1456 $cm^{-1}$ as a function of cinchonidine concentration in solution. A comparison is made with the analogous signal observed on $Pt/Al_2O_3$ at 1458 $cm^{-1}$ (see Ref. (15) and Table 1). The solid line is a fit of the data assuming a Langmuir-like adsorption.

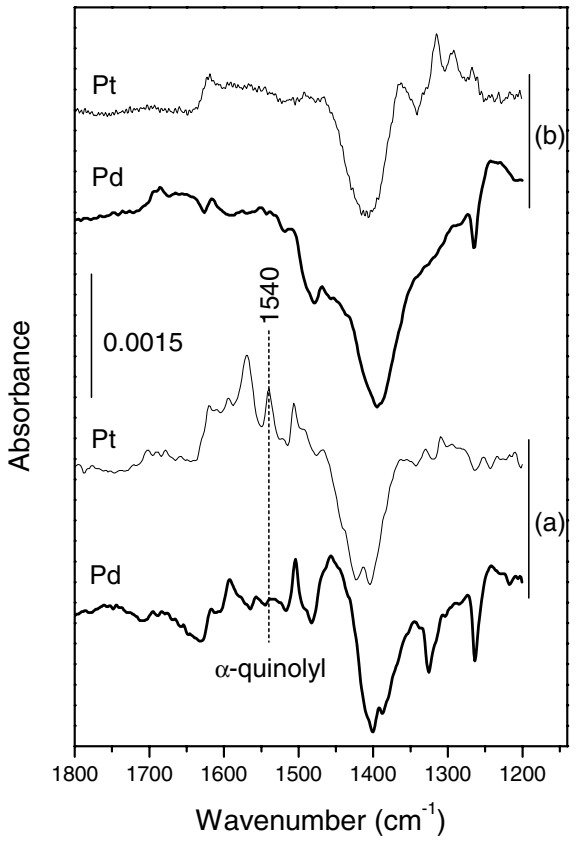


**FIG. 7.** *In situ* ATR spectra of (a) quinoline and (b) 2-methylquinoline adsorption from $H_2$-saturated $CH_2Cl_2$ solvent on $Pd/Al_2O_3$ and $Pt/Al_2O_3$ at 283 K. The concentration of the solutions was set at $10^{-4}$ and $10^{-3}$ M for adsorption on Pd and Pt, respectively. The position of the signals corresponding to the $\alpha$-quinolyl species on $Pt/Al_2O_3$ is also highlighted.

$Pd/Al_2O_3$ model catalyst at 283 K and served as reference for the assignment of the observed signals of cinchonidine and for the determination of the orientation of the adsorbed species. *In situ* ATR spectra are shown in Fig. 7, together with the corresponding spectra on $Pt/Al_2O_3$ for comparison. The difference between quinoline adsorbed on Pt and Pd is obvious. Besides the set of signals (1615, 1590, and 1506 $cm^{-1}$) similar to cinchonidine, a strong signal at around 1456 $cm^{-1}$ was observed on Pd, whereas the signal at 1590 $cm^{-1}$ displayed a shoulder at ~1570 $cm^{-1}$, which is, on the other hand, the most prominent band on Pt. Although the IR spectrum of quinoline possesses a weak vibration at 1469 $cm^{-1}$ (~1463 $cm^{-1}$ for cinchonidine; Table 1) (15), this is absent or at least less obvious on Pt (Fig. 7). We suggest that this band does not entirely belong to quinoline and that part of the signal arises from the continued cleaning of the metal surface, producing O-containing fragments (alkoxy groups). Comparison between the spectra of cinchonidine adsorbed on Pd and Pt supports this conclusion. In fact, the signal at 1458 $cm^{-1}$ on Pt is less intense than on Pd and is clearly composed of two bands on Pd. It must be noted that in all adsorption measurements the $H_2$ cleaning period was restricted to 10 min. Figure 2 shows that afterwards, however, the process continues slowly.

As for pyridine and quinoline, Fig. 7 clearly shows that the $\alpha$-quinolyl species, whose typical signal is indicated by a dashed line, is absent on Pd.

The ATR spectra of 2-methylquinoline on $Pd/Al_2O_3$ did not show any quinoline signals except for a very weak band at 1510 $cm^{-1}$, which disappeared with the following $H_2$ flow. However, negative features found at around 1400 and 1264 $cm^{-1}$ clearly show that 2-methylquinoline adsorbs on Pd. The molecular plane of 2-methylquinoline is believed to orient preferentially parallel to the surface, with the methyl group hindering the interaction between the quinoline *N* and the metal, in agreement with the absence of clear quinoline vibrations. A relatively broad signal was again observed at around 1540 $cm^{-1}$.

*Effect of cinchonidine adsorption.* It is obvious from Figs. 3 and 5 that the adsorption process also induces the displacement of some species from the solid–liquid interface. The signal found at 1324 $cm^{-1}$ which is accompanied by a signal at around 1090 $cm^{-1}$ (not shown in Fig. 5) matches the shoulder of the signal at 1392 $cm^{-1}$ observed in Fig. 2. These signals are attributed to ethylidyne ($\equiv C–CH_3$), which is stable at this temperature (39) and originates from recombination of $CH_x$ fragments formed from $CH_2Cl_2$ decomposition on clean Pd. These have been observed also for the $Pt/Al_2O_3$ model system. The frequency exhibited on Pd is reasonably close to that found for single-crystal (39) and supported Pd (40) and demonstrates that the signals observed at 1338 and 1120 $cm^{-1}$ on Pt are due to ethylidyne (14, 15, 20). The displacement of hydrocarbon fragments $CH_x$ and $\equiv C–CH_3$, absorbing at ~1390 and 1324 $cm^{-1}$, respectively, and solvent (negative signal at 1264 $cm^{-1}$) indicates that the chiral modifier as well as pyridine, quinoline, and 2-methylquinoline have to compete with other species for adsorption onto the metal surface.

For comparison with the CO found upon adsorption of cinchonidine on $Pt/Al_2O_3$ (15) and according to the recent observation that CO can display unusual frequencies if adsorbed at metal–support interfacial sites (41), the broad signal at 1735 $cm^{-1}$ together with that at ~1680 $cm^{-1}$ can be assigned to adsorbed CO, as mentioned above.

A weak signal at around 1540 $cm^{-1}$ can also be observed. This signal has also been detected in the spectra shown in Fig. 3 and was also found for pyridine, quinoline, and 2-methylquinoline adsorption. Therefore, it cannot be assigned to a species arising from adsorption of cinchonidine on palladium. We tentatively assign it to hydrocarbon or O-containing species.

## DISCUSSION

STM measurements together with *in situ* ATR–IR spectroscopy clearly demonstrate that the treatment of the

$Pd/Al_2O_3$ thin film with dissolved hydrogen leads to dramatic changes in the spectra and film morphology. It is well-known that adsorbates such as CO can induce reconstruction of the Pd surface (42, 43). The surface cleaning, as followed by ATR spectroscopy, accompanies the large modification of the metal surface. This observation supports our conclusion drawn for the $Pt/Al_2O_3$ model catalyst, where hydrogen was proposed to be responsible for the observed changes in the ATR spectra and film morphology (20). From a chemical point of view, hydrogen removes the contamination film, composed mostly of carbonates and hydrocarbons, covering the metal surface. Exposition of the cleaned Pd induces decomposition of the solvent and consequently formation of a different adsorbate layer. In the case of $CH_2Cl_2$ solvent this layer consists of $CH_x$ and $\equiv C–CH_3$ species. This becomes relevant for adsorption studies.

A phenomenon intimately associated with the presence of hydrogen and the film reconstruction is the absorption enhancement (compare Figs. 3A and 3B). Figure 3B shows that CO adsorbs slowly also when Pd is not treated with $H_2$. The increase in the Pd particle size subsequent to hydrogen admission results in a sudden increase in the intensity of the signals associated with CO. Considering that the new signals arise from the same amount of CO, it becomes obvious that metal particle size and signal intensity are closely related, as was found for the surface-enhanced infrared absorption (SEIRA) effect (44). Moreover, the enhancement is accompanied by a change in the shape of the IR signal of CO, which has been discussed for the Pt and $Pt/Al_2O_3$ films (20, 31). We have shown that, depending on the optical constants of the Pt film, vibrational bands of strong absorbers can become considerably distorted. As demonstrated above, the ATR spectra of cinchonidine also display a remarkable enhancement effect in comparison to the spectra obtained on Pt. Compared to the signals of cinchonidine on Pt (Fig. 5) the signals are enhanced by a factor of 3 on Pd, in agreement with the results reported for CO. This is in agreement with the larger particle size observed for Pd compared to Pt. It should be noted that the thickness of the Pd thin film is twice that of Pt.

Since the adsorption of CO and pyridine from $CH_2Cl_2$ solvent on the $Pd/Al_2O_3$ thin films gave results similar to that on commercial supported Pd-based catalysts the evaporated films can be considered as promising model catalysts. CO was found to adsorb both on top and multibonded (more likely in threefold coordination) (30) whereas pyridine was mostly oriented with the molecular plane tilted away from the metal surface.

The adsorption of the chiral modifier cinchonidine on $Pd/Al_2O_3$ model catalysts has been studied *in situ* similarly to the recently reported adsorption on $Pt/Al_2O_3$. It should be noted that owing to the relatively low concentration of cinchonidine ($10^{-4}$ M) the signals observed in Fig. 5 correspond to adsorbed cinchonidine and not to the alkaloid in solution. Cinchonidine adsorption on Pd at 283 K in the presence of dissolved hydrogen is both time and coverage dependent, as is illustrated in Figs. 5 and 6. For comparison with quinoline and pyridine under the same experimental conditions, adsorption of the alkaloid is dictated by the quinoline moiety. Cinchonidine adsorbs intact on Pd and there is no indication that the quinuclidine moiety takes part in the adsorption, whereas the vinyl group is readily hydrogenated at 283 K. These findings have been reported also for cinchonidine on Pt (15). Three differently adsorbed species have been observed for cinchonidine on $Pt/Al_2O_3$. In the first species the quinoline moiety is approximately parallel to the surface ($\pi$-bonding, labelled **1**), whereas in the second species a Pt–C $\sigma$-bond is formed by $\alpha$-H abstraction ($\alpha$-quinolyl, **2**). The third species, weakly adsorbed, bonds to the surface through the *N* lone pair of the quinoline moiety (**3**) and exhibits a solution-like spectrum.

Figure 6, and to a lesser extent Fig. 5, demonstrates that at least two species of adsorbed cinchonidine can be found on the Pd surface. One species is associated with the band at 1567 $cm^{-1}$ and the other with bands at 1612, 1586, and 1509 $cm^{-1}$, similar to what was found on Pt (15). The ATR spectra shown in Fig. 6, which do not display signals of solution-like cinchonidine at low coverage, suggest that cinchonidine adsorbs at low coverage with the quinoline ring nearly flat, i.e., through $\pi$-bonding between the quinoline moiety and the metal. In addition, since the absorbance of the signal at 1567 $cm^{-1}$ remains approximately constant after about $10^{-5}$ mol/L whereas the signal at 1586 $cm^{-1}$ increases, it seems that there is no interconversion taking place between the two species. As the surface gets more crowded additional cinchonidine molecules adsorb with the quinoline ring tilted with respect to the metal surface, through the quinoline *N*. It will become clear through the analysis of some details that this process is slightly different from that on Pt.

Considering that the signal at 1509 $cm^{-1}$ follows the behaviour of the signal at 1586 $cm^{-1}$ (Figs. 5 and 6), the two observed species on Pd can be assigned following the notation introduced for cinchonidine on $Pt/Al_2O_3$ (15). A first (nearly parallel adsorbed) species (labelled **1′**) corresponds to species **1** on Pt, whereas the second (tilted, **3′**) resembles species **3** on Pt. Species **1′** is characterised by the signal at 1567 $cm^{-1}$, whereas species **3′** corresponds to the signals at 1612, 1586, and 1509 $cm^{-1}$. In addition, both species bear the signal at 1456 $cm^{-1}$ associated with the quinuclidine moiety. Species **3′** possibly also contributes to the signal at ~1570 $cm^{-1}$. Table 1 summarises the assignment. Normal modes and dynamic dipole moments of the discussed vibrations have previously been reported (15). Significantly, the ATR spectra do not present any indication of a species where the $\alpha$-H to the quinoline *N* has been removed and a covalent C–Pd bond formed, in contrast to Pt (i.e., species **2**). This is in good agreement with the results of pyridine and

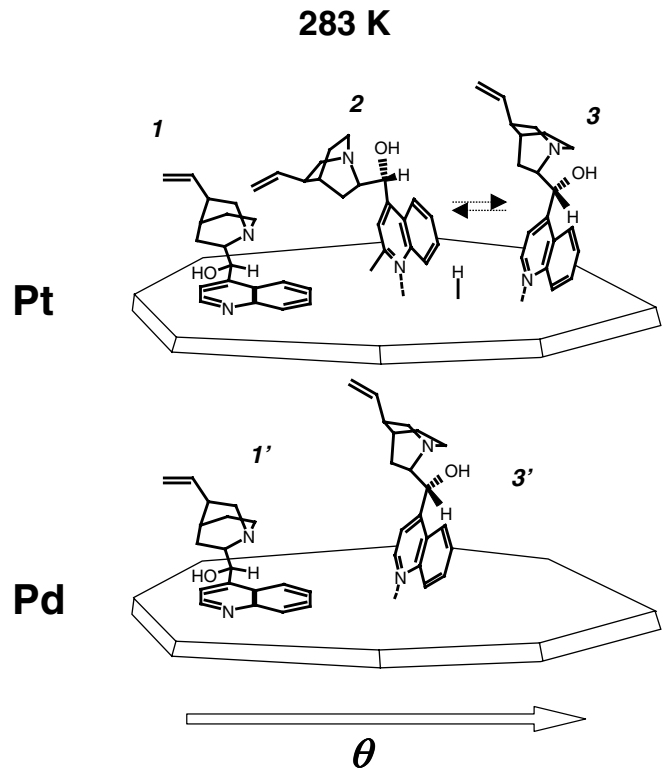


**FIG. 8.** Pictorial representation of the surface species of cinchonidine on $Pd/Al_2O_3$ and $Pt/Al_2O_3$ model catalysts at 283 K. The evolution of the species is coverage ($\theta$) dependent. See text for nomenclature. No specific crystallographic plane is intended with the graphical representation of the metal surface.

quinoline adsorption (Figs. 4 and 7). Figure 8 summarises the surface species of cinchonidine observed on both metals in the presence of hydrogen as a function of surface coverage.

We exclude now species **2** from the discussion because it is found exclusively on Pt. There are two specific features in the spectra presented in Figs. 5 and 6 suggesting that the interaction between cinchonidine and Pd is weaker than the interaction between cinchonidine and Pt. Consequently, the observed adsorbed species of cinchonidine on Pd behave slightly differently than on Pt. Spectra at high cinchonidine coverage on Pd (bold lines in Figs. 5 and 6) much resemble the solution spectrum of cinchonidine, more than do the spectra recorded on the Pt thin films. On adsorption the molecular vibrations are less perturbed on Pd than on Pt. Also, Fig. 5 shows that cinchonidine is almost completely removed when flowing hydrogen-saturated solvent over the sample. Desorption is also observed on Pt (15), but species **1** and **2** are still clearly visible on Pt during the desorption step, in contrast to species **1**′ on Pd. What is more important is that the IR spectrum of the adsorbed species on Pt looks different from the solution spectrum because of species **1** and **2** (Fig. 5). The same observation holds for quinoline (Fig. 7). The intensity ratio between the signal at around 1590 $cm^{-1}$ and that at around 1570 $cm^{-1}$ is particularly striking: Passing from one metal to the other the intensity ratio is reversed. This means that species **1** contributes more significantly to the signal at 1570 $cm^{-1}$ for cinchonidine on Pt. This indicates that the relative abundance of species **1** to species **3** on Pt is higher than that corresponding to species **1**′ and **3**′ on Pd.

Comparison of the time and concentration dependence of the spectrum on the two metals suggests that species **3**′ already appears on Pd at a relatively low coverage, i.e., earlier, than species **3** on Pt. Comparison of the intensity of the signal at ~1570 $cm^{-1}$ on Pd and Pt with that at around 1590 $cm^{-1}$ agrees with this observation. Hence, although both bonding modes are observed, there is evidence that the flat species (**1** and **1**′) are more favoured on Pt than on Pd, whereas the tilted species (**3** and **3**′) are preferred on Pd. Species **1** is more abundant on Pt than species **1**′ on Pd at similar cinchonidine coverage. The fact that cinchonidine does not form the $\alpha$-quinolyl species (**2**) on Pd (neither does pyridine or quinoline) further indicates that the bonding of the alkaloid is weaker to Pd than to Pt.

The different stability of the observed species of cinchonidine on the two metals must be due to different adsorbate–metal interactions. Pt and Pd have similar interatomic distances, the same number of valence electrons, and similar work functions. Despite these similarities the interaction of unsaturated hydrocarbons with the two metals is quite different (38) and so is the chemistry of hydrocarbons. An important difference between the two metals is the diffuseness of the 5d orbitals of Pt and the 4d orbitals of Pd, which is much larger in the former case. The d orbitals play a dominant role in the adsorbate bond. The larger diffuseness of the Pt 5d orbitals leads to larger orbital overlap with the adsorbate orbitals and hence to stronger adsorbate bonds compared to Pd. A stronger adsorbate bond also leads to a larger distortion of the adsorbate intramolecular potential energy surface and hence to larger shifts in the vibrational frequencies with respect to the undistorted free molecule. The stronger bonding of unsaturated hydrocarbons and their larger shifts in vibrational frequencies for Pt as compared to Pd have been demonstrated, for example, for benzene, toluene, and pyridine (38). Our results, which indicate that cinchonidine is more strongly adsorbed on Pt than on Pd and that its vibrational modes are shifted more with respect to the free molecule on Pt than on Pd (Table 1), agree with this general trend.

The different H/D exchange behaviour of 10,11-dihydrocinchonidine (DHC) on Pd and Pt (45) supports the slightly different relative stability of the surface species of cinchonidine on the two metals. On Pt, H/D exchange has been reported to occur at all positions of the quinoline ring, predominantly in the position $\alpha$ to the quinuclidine *N* and at the carbon ($C_8$) located on the second ring

symmetric to the quinoline *N*. On Pd, *only* hydrogen at the latter two positions was shown to exchange to some extent. This agrees well with a preferred interaction through the quinoline *N* more than with the $\pi$-electrons and with the quinoline moiety standing away from the Pd surface. Pt shows a behaviour similar to Pd only when increasing the temperature from 293 to 333 K, which is supposed to lead to the tilting of the aromatic ring as observed by NEXAFS (12). Moreover, the hydrogen in the position $\alpha$ to the quinoline *N* exchanges approximately three times less on Pd than on Pt (30 vs 94%) at 293 K, in agreement with the lack of $\alpha$-quinolyl species in the ATR spectra of cinchonidine on Pd at 283 K. In agreement with our ATR measurements, these results suggest that the interaction of cinchonidine is weaker with Pd than with Pt. The relative abundance of cinchonidine with the quinoline moiety parallel ($\pi$-bonded) and tilted ($\sigma$-bonded) with respect to the surface is shifted in favour of the latter when going from Pt to Pd.

The weaker adsorption of the cinchonidine modifier in the $\pi$-bonded mode on Pd than on Pt may explain why typically a higher modifier to the reactant ratio is needed in the former case to induce optimal enantiodifferentiation in the heterogeneous enantioselective hydrogenation on the two metals (7, 8).

The comparative study of cinchonidine adsorption on $Pd/Al_2O_3$ and $Pt/Al_2O_3$ indicates that on both metals the adsorption mode is fairly similar, at least in the absence of interacting substrates (reactants). In any case, the subtle differences in the adsorption behaviour cannot explain the vastly different behaviour of *cinchona*-modified platinum and palladium catalysts, which has clearly to be traced to the different intrinsic catalytic properties of these metals.

## CONCLUSIONS

The adsorption of pyridine, quinoline, 2-methylquinoline, and cinchonidine on $Pd/Al_2O_3$ model catalysts has been investigated. The model catalysts were prepared by physical vapour deposition and characterised by XPS, STM, and IR spectroscopy. Hydrogen treatment induced morphological changes which were followed by STM and *in situ* ATR–IR spectroscopy. Similarly to the $Pt/Al_2O_3$ model system, infrared absorption enhancement has been observed also for Pd. Both CO and cinchonidine display signals more intense by a factor of 3 with respect to Pt.

Adsorption of the chiral auxiliary has been studied at 283 K and compared with the results obtained recently for the $Pt/Al_2O_3$ model catalyst. So far, no *in situ* spectroscopic study of the adsorption of cinchonidine on palladium has been reported. Consistent with the time and coverage dependence of the signals of adsorbed cinchonidine, two main species have been identified on Pd and have been assigned according to the species observed on Pt. A species with the quinoline moiety predominantly parallel to the surface, interacting with the $\pi$-electrons of the quinoline moiety, and a species interacting with Pd through the lone pair of the quinoline *N* are observed. Compared to Pt, the relative abundance of the two species under similar conditions is different on the two surfaces, such that the $\pi$-bonded species is less stable on Pd than on Pt. Based on the comparison with adsorbed pyridine on Pd and Pt, the most obvious difference in the adsorption of cinchonidine on the two metals is that the $\alpha$-quinolyl species observed on Pt is absent on Pd. The difference in the diffuseness of the d orbitals of the metal is likely at the origin of the different behaviour with respect to the adsorption of cinchonidine.

## ACKNOWLEDGMENTS

The authors gratefully acknowledge the financial support from the Swiss National Science Foundation and ETH Zurich.

## REFERENCES

1. Centi, G., *J. Mol. Catal. A* **173**, 287 (2001).
2. Blaser, H. U., Indolese, A., Schnyder, A., Steiner, H., and Studer, M., *J. Mol. Catal. A* **173**, 3 (2001).
3. Nitta, Y., Ueda, Y., and Imanaka, T., *Chem. Lett.* 1095 (1994).
4. Borszeky, K., Mallat, T., and Baiker, A., *Catal. Lett.* **41**, 199 (1996).
5. Borszeky, K., Mallat, T., and Baiker, A., *Catal. Lett.* **59**, 95 (1999).
6. Borszeky, K., Bürgi, T., Zhaohui, Z., Mallat, T., and Baiker, A., *J. Catal.* **187**, 160 (1999).
7. Huck, W. R., Mallat, T., and Baiker, A., *J. Catal.* **193**, 1 (2000).
8. Huck, W. R., Bürgi, T., Mallat, T., and Baiker, A., *J. Catal.* **200**, 171 (2001).
9. Huck, W. R., Mallat, T., and Baiker, A., *N. J. Chem.* **26**, 6 (2002).
10. Tungler, A., Nitta, Y., Fodor, K., Farkas, G., and Máthé, T., *J. Mol. Catal. A* **149**, 135 (1999).
11. Carley, A. F., Rajumon, M. K., Roberts, M. W., and Wells, P. B., *J. Chem. Soc. Faraday Trans.* **91**, 2167 (1995).
12. Evans, T., Woodhead, A. P., Gutiérrez-Sosa, A., Thornton, G., Hall, T. J., Davis, A. A., Young, N. A., Wells, P. B., Oldman, R. J., Plashkevych, O., Vahtras, O., Ågren, H., and Carravetta, V., *Surf. Sci.* **436**, L691 (1999).
13. Bonello, J. M., Sykes, E. C. H., Lindsay, R., Williams, F. J., Santra, A. K., and Lambert, R. M., *Surf. Sci.* **482–485**, 207 (2001).
14. Ferri, D., Bürgi, T., and Baiker, A., *J. Chem. Soc. Chem. Commun.* 1172 (2001).
15. Ferri, D., and Bürgi, T., *J. Am. Chem. Soc.* **123**, 12074 (2001).
16. Harrick, N. J., *in* "Internal Reflection Spectroscopy," Interscience, New York, 1967.
17. Kubota, J., and Zaera, F., *J. Am. Chem. Soc.* **123**, 11115 (2001).
18. Baiker, A., *J. Mol. Catal. A* **163**, 205 (2000).
19. Bonello, J. M., Lindsay, R., Santra, A. K., and Lambert, R. M., *J. Phys. Chem. B* **106**, 2672 (2002).
20. Ferri, D., Bürgi, T., and Baiker, A., *J. Phys. Chem. B* **105**, 3187 (2001).
21. Briggs, D., and Seah, M. P., Ed., "Practical Surface Analysis," Vol. 1. Wiley, New York, 1990.
22. Jones, M. G., Nevell, T. G., Ewen, R. J., and Honeybourne, C. L., *Appl. Catal.* **70**, 277 (1991).
23. Wolf, E. E., *Top. Catal.* **13**, 21 (2000).
24. Schildenberger, M., Prins, R., and Bonetti, Y. C., *J. Phys. Chem. B* **104**, 3250 (2000).
25. Solymosi, F., and Rasko, J., *J. Catal.* **155**, 74 (1995).
26. Davis, J. L., and Barteau, M. A., *Surf. Sci.* **235**, 235 (1990).

27. Ataka, K., and Osawa, M., *Langmuir* **14**, 951 (1998).
28. Zippel, E., Breiter, M. W., and Kellner, R., *J. Chem. Soc. Faraday Trans.* **87**, 637 (1991).
29. Bradshaw, A. M., and Hoffmann, F. M., *Surf. Sci.* **72**, 513 (1978).
30. Vannice, M. A., Wang, S. Y., and Moon, S. H., *J. Catal.* **71**, 152 (1981).
31. Bürgi, T., *Phys. Chem. Chem. Phys.* **3**, 2124 (2001).
32. Haq, S., and King, D. A., *J. Phys. Chem. B* **100**, 16957 (1996).
33. Di Nardo, N. J., Avouris, P., and Demuth, J. E., *J. Chem. Phys.* **81**, 2169 (1984).
34. Johnson, A. L., Muetterties, E. L., Stöhr, J., and Sette, F., *J. Phys. Chem.* **89**, 4071 (1985).
35. Grassian, V. H., and Muetterties, E. L., *J. Phys. Chem.* **90**, 5900 (1986).
36. Mate, C. M., Somorjai, G. A., Tom, H. W. K., Zhu, X. D., and Shen, Y. R., *J. Chem. Phys.* **88**, 441 (1988).
37. Jakob, P., Lloyd, D. R., and Menzel, D., *Surf. Sci.* **227**, 325 (1990).
38. Grassian, V. H., and Muetterties, E. L., *J. Phys. Chem.* **91**, 389 (1987).
39. Kesmodel, L. L., and Gates, J. A., *Surf. Sci.* **111**, L747 (1981).
40. Beebe, T. P., Albert, M. R., and Yates, J. T., *J. Catal.* **96**, 1 (1985).
41. Ferri, D., Bürgi, T., and Baiker, A., *Phys. Chem. Chem. Phys.* **4**, 2667 (2002).
42. Raval, R., Haq, S., Harrison, M. A., Blyholder, G., and King, D. A., *Chem. Phys. Lett.* **167**, 391 (1990).
43. El-yakhloufi, M. H., and Gillet, E., *Catal. Lett.* **17**, 11 (1993).
44. Osawa, M., Ataka, K. I., Yoshii, K., and Nishikawa, Y., *Appl. Spectrosc.* **47**, 1497 (1993).
45. Bond, G., and Wells, P. B., *J. Catal.* **150**, 329 (1994).